Conveyor System with a Highly Integrated Permanent Magnet Gear and Motor

Nielsen, Simon Staal; Holm, Rasmus Koldborg; Rasmussen, Peter Omand

Published in:
IEEE Transactions on Industry Applications

DOI (link to publication from Publisher):
10.1109/TIA.2020.2977877

Publication date:
2020

Document Version
Accepted author manuscript, peer reviewed version

This article has been accepted for publication in a future issue of this journal, but has not been fully edited. Content may change prior to final publication. Citation information: DOI 10.1109/TIA.2020.2977877, IEEE Transactions on Industry Applications

Conveyor System with a Highly Integrated Permanent Magnet Gear and Motor

1st Simon Staal Nielsen
Department of Energy Technology
Aalborg University
Aalborg, Denmark
ssn@et.aau.dk

2nd Rasmus Koldborg Holm
Department of Energy Technology
Aalborg University
Aalborg, Denmark
rkh@et.aau.dk

3rd Peter Omand Rasmussen
Department of Energy Technology
Aalborg University
Aalborg, Denmark
por@et.aau.dk

***Abstract*—Magnetic gears have attracted increasing attention in recent years due to many possible advantages over mechanical gears. Many papers have been presented with theoretical proof of the basic properties and topologies of the magnetic gears and their parallels to mechanical counterparts, however, very little work has been done to implement the magnetic gears into actual applications which fully utilises their desirable properties. This paper presents a concept study and physical demonstrator of a magnetic gear and permanent magnet machine highly integrated into a drive unit for chain conveyor systems. Several current mechanical gear/motor combinations are replaced by the new drive unit, which is more compact and potentially more energy efficient. Moreover, the inherent overload protection of the magnetic gear eliminates the need for a mechanical slip clutch in the system, further reducing system complexity and improving reliability. An experimentally measured torque density of 142 Nm/l is obtained for the active magnetic gear volume.**

***Index Terms*—Conveyor, drive unit, industrial application, integration, magnetic gear, torque density**

I. Introduction

During the last 15 years the magnetic gears (MGs) have turned into quite a hot topic in academia due to its many advantages of no mechanical wear, physical isolation of load from drive (which can be exploited in e.g. pump applications), reduced maintenance, potentially good efficiency, inherent overload protection, reduced acoustic noise from mechanical contact, and the absence of backlash. Even so MGs have been a known technology the whole 20th century its potential was first made clearly visible in the paper [1] where a theoretical calculated torque density of 100 Nm/l was presented. The paper uses the wording novel in its title which can be considered unfair since the presented topology was exactly the same as the one described by T.B Martin in a patent from 1968 [2]. At that time, strong rare earth magnets were not available making the torque density of the MG impractical for a more widespread use of the technology at that time. In the early years of the technology the focus was mainly to describe the basic functionality, making demonstrators to prove the principle, compare it to conventional gears, presenting different topologies etc., [1] [3] [4] [5] [6] [7] [8] [9]. Since the MG to a very large extent will/can be driven by electrical machines, and the research and the basics of these machines has been covered extensively, many turned into looking to combine/integrate the MG and electric machine. Several papers in that area saw its daylight, [10] [11] [12], while the research of understanding more of its details in form of optimisation, cogging torque, 3D effect etc. continued. Even though a lot of academic work is done in the field, the real commercial breakthrough has not arrived although it could have been expected. The delay may be attributed to recent sky-high magnet costs, and also likely to the fact that the technology has not been demonstrated in real, highly relevant applications. For instance, in [13] very good results were shown in terms of energy efficiency and torque density, but the implementation had drawbacks as solid steel was used for the segments. The result is an operating speed too low for other than a few, very specialised applications. In the other end [14] presents a motor integrated permanent magnet gear (MIPMG) for a traction application. This MG and motor combination runs at very high speed which leads to large rotational losses. Although a large amount of work has been done to reduce these losses, and better results were obtained, the cost of the MG and motor also increased. If the range between the two examples is considered, several applications which fit the MG very well can be found. One example is conveyor belts where the speed is more appropriate, and the special properties of the MG such as the inherent overload protection, high torque density, minimal maintenance and potentially high energy efficiency are perfect matches.

This paper presents a highly integrated implementation of the MG into a chain conveyor application. The MG is driven by a permanent magnet synchronous machine (PMSM) and three different configurations are discussed. Both design, physical tests and evaluation of the system is presented. The aim is to replace the existing drive unit with a more efficient and compact drive unit, which also replaces several current combinations of line fed induction machines and mechanical gearboxes covering the speed and torque ranges required by customers. Furthermore, this paper contributes to link the extensive academic activities in the MG area to actual industrial applications. Section 2 discusses the topology of the MG and PMSM configuration and section 3 describes the development of the demonstrator. In section 4 the test results and evaluation of the MG and PMSM are given, and finally, the conclusion is given in section 5. An earlier version of this paper was presented on the 2018 IEEE Energy Conversion Congress and Exposition (ECCE) [15].

TABLE I
MAIN CONSTRAINTS AND REQUIREMENTS FOR THE DRIVE UNIT.

Max sprocket speed [rpm]	298
Peak sprocket torque [Nm]	100
Nominal sprocket torque (0-12.4 rpm) [Nm]	80.9
Nominal sprocket torque (149-298 rpm) [Nm]	22.7
Max power @ 298 rpm [W]	708
Drive unit width, excl. gear/motor [mm]	85
Max sprocket center diameter [mm]	105
Max diameter of external components [mm]	150
Cooling method	Natural
Target gear ratio	15:1
IP rating	IP65

II. TOPOLOGY OF MG AND PMSM COMBINATION

The new drive unit must fit into a current conveyor system which inevitably introduces some constraints on the system design, such as specific outer dimensions and mechanical interface to conveyor chains. In fig. 1 the current drive unit is seen. It mainly consists of two aluminium flanges holding a polymer sprocket on a shaft to drive the conveyor chain. An external drive comprised of a motor/gear combination and optionally a frequency converter is attached to the 120 mm long shaft to drive the sprocket.

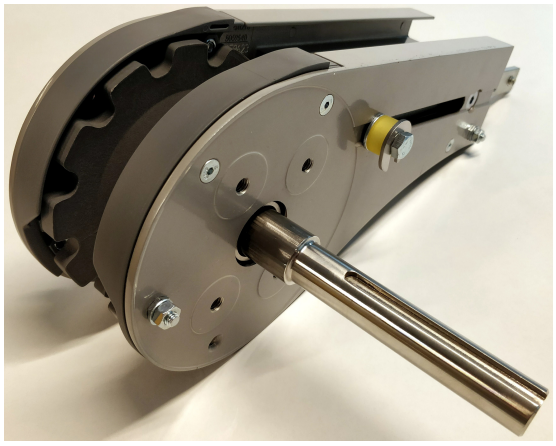

Fig. 1. Current drive unit with polymer sprocket on a shaft, to which an external motor/gearbox combination can be attached.

The new drive unit can only utilise passive cooling, hence all losses must be dissipated mainly through the aluminium flanges and the units own housing. In table I the specifications for the drive unit are outlined.

The target gear ratio is chosen as a compromise between maximum frequencies and the torque requirement of the PMSM. If the rule of thumb for volumetric torque densities of MGs (100 Nm/l) and naturally cooled PMSMs (10 Nm/l) are examined, there is approximately a factor of 10 in favor of the MGs. Hence, to somehow balance the volumetric size of MG and PMSM, there should be a gear ratio of at least 10. For the MG topologies with an integrated PMSM, the system may benefit from an even higher gear ratio, as this lowers the torque requirements for the PMSM, which is almost thermally isolated inside the MG and will face difficulties to get rid of the heat generated by losses. The price paid for higher gear ratios is higher frequencies which increases the challenging core- and magnet losses. With a gear ratio of 15:1, the maximum speed of the PMSM is 4470 rpm. The peak torque requirement is 6.7 Nm and the maximum continuous torque is 5.4 Nm.

The development of the drive unit is divided into two primary stages, where the first stage is used to chose the topology of the MG and motor combination. In this stage, the MGs are designed via 2D Finite Element Analysis (FEA) parameter sweeps, and the PMSMs are approximately sized via general sizing rules and motor data from reputable PMSM manufacturers. The topologies which have been considered for the drive unit can be divided into three main types:

(a) Fully integrated, MG is inside sprocket, PMSM is integrated into MG (fig. 2a).
(b) External, MG and PMSM is on side of drive unit and designed as an MIPMG (fig. 2b).
(c) Semi integrated, MG is inside sprocket, PMSM is placed on side of unit (fig. 2c).

All three topologies have been through several design iterations regarding mechanical integration. Cross sections of the three solutions from the first stage in fig. 2 are shown in proportion with dimensions in millimeters.

In the fully integrated version, the segment ring is kept stationary, and the sprocket is mounted to the low speed (LS) rotor. The high speed (HS) rotor magnets share back iron with the rotor magnets of the integrated PMSM. This topology has been deemed unfeasible early in the process, despite the very appealing compact form which is the shortest of the three. The gearing ratio is limited to 12:1 due to the size of the magnets and the requirement of a Halbach arrangement of the magnets on the LS rotor to obtain the required torque. This gearing ratio requires a torque density of 27 Nm/l for the passively cooled PMSM which is not manageable for such a small machine which is fully enclosed in the MG. Furthermore, the thermal coupling between MG and PMSM requires a grade of magnets which are rated for higher temperature as the PMSM is pushed very hard.

The external topology has the advantage of a larger diameter and uses the segment ring as output rotor, which increases the gear ratio and torque density. In this particular implementation it is the volume of the internal PMSM that defines the minimum volume of the combined PMSM and MG. The result is a small required torque density for the MG compared to topology a) and c). For this reason, a Halbach magnet array on the LS rotor is not necessary, making this component more simple. Furthermore, this topology makes it easy to obtain the required IP65 rating, as the LS rotor is stationary. The low speed output shaft is easily sealed with a radial shaft seal. The flanges and sprocket can be reused from the existing drive unit. The disadvantages of this topology includes the thermal coupling between MG and PMSM, forces which are transferred through the segment ring and a cup-rotor for the HS rotor / PMSM rotor. The space inside the sprocket is not utilised and the structure placed external to the 85 mm width

This article has been accepted for publication in a future issue of this journal, but has not been fully edited. Content may change prior to final publication. Citation information: DOI 10.1109/TIA.2020.2977877, IEEE Transactions on Industry Applications

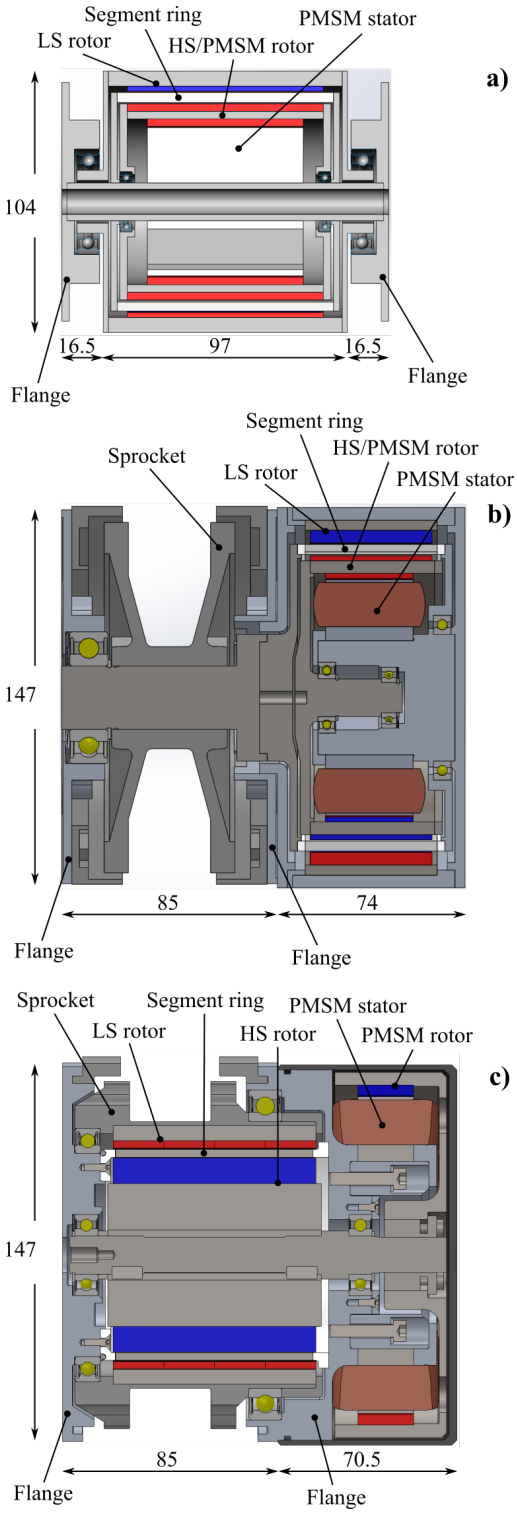

Fig. 2. Fully integrated (a), external (b) and semi integrated (c) topologies. Dimensions are given in mm.

of the main unit are the widest. It should be mentioned, that the illustration of topology b) in fig. 2 has not been through a detailed design phase. A known parameter which would make the final design wider is the space for end windings, at least 8 mm would be added for this reason alone. Also, motor wires must be taken out on the right side of the MIPMG. This increases the effective width of the solution.

The semi integrated version utilises the space inside the sprocket for the MG. The segment ring is fixed, and the sprocket is mounted to the LS rotor. The HS rotor shares shaft and bearings with the PMSM rotor, which is an outer rotor machine. This topology introduces a thermal decoupling of the MG and PMSM, hence the magnet grade of the MG regarding temperature primarily depends on the losses of the MG, and the PMSM may be pushed harder. A better thermal contact can be made to the stator of the PMSM compared to topology a) and b), and the windings are easily accessible for wiring to the inverter through the aluminium flange where the PMSM is mounted. The external placement of the PMSM makes it possible to obtain maximum possible air gap diameter for the given envelope of 150 mm diameter. Finally, this topology does not transfer any load through the segment ring other than the MG torque, and it is mechanically simple. The disadvantages of the topology includes that no existing drive unit components can be reused, large bearings are used which tends to be more expensive compared to some of the bearings used in the other topologies and the design freedom of the MG is reduced compared to the fully external solution.

The semi integrated solution is chosen. There are few disadvantages to the topology, and they are small compared to the advantages obtained.

III. Developing the Demonstrator

The detailed design of the MG and PMSM is carried out as an iterative process with parameter sweeps. Due to the decoupling between the MG and PMSM, the two designs are made separately. The HS rotor is designed with 2 pole pairs. This choice has been made to reduce the flux frequency in the MG laminations and to take the constrain on the outer diameter of the MG into account, which causes too small magnets at higher HS pole count at the desired gear ratio when considering mechanical integrity, manufacturability and flux leakage. With 2 HS pole pairs, the 15:1 gear ratio is obtained with 32 segments and 30 LS pole pairs. The steel segments are connected with a thin bridge as shown in fig. 3 that improves the segment ring in two areas. Firstly, the bridge has been introduced before in literature to improve upon mechanical strength and the handling of the segments [11] [16] and secondly, the bridge reduces the space harmonics of the flux seen by the HS magnets which reduces the eddy current losses induced in these [11] [17].

The primary objective of the parameter sweeps is torque density, although, at the same time, manufacturability is important as the drive unit must be feasible in a commercial context. The parameter sweep of the MG is divided into three stages. First, the major dimensions are swept, being radial magnet thickness, radial back iron thickness and radial segment height. In the second stage, the segment ratio is swept, which defines the relationship between the width of segments and air between the segments, and in the last stage, the HS magnet ratio and the radial thickness of the bridge connecting the steel

This article has been accepted for publication in a future issue of this journal, but has not been fully edited. Content may change prior to final publication. Citation information: DOI 10.1109/TIA.2020.2977877, IEEE Transactions on Industry Applications

segments is swept. Finally, demagnetisation is investigated by shifting the LS rotor 1 pole which is the most critical position with respect to demagnetisation of the LS magnets. To include the influence of end-effects on the MG, the final MG is modeled in 3D FEA. Final specifications of the MG are seen in table II and the cross section of the MG is seen in fig. 3.

TABLE II
FINAL DIMENSIONS OF MG.

HS pole pairs	2
Nr. of segments	32
LS pole pairs	30
HS radial magnet thickness [mm]	10
HS back iron thickness [mm]	21
LS radial magnet thickness [mm]	3
LS back iron thickness [mm]	5
Segment radial thickness [mm]	3
Segment ratio [-]	0.55
Segment bridge thickness [mm]	0.5
Magnet grades HS/LS	N4520/N4025
HS and LS air gap [mm]	0.4
Stack length, HS + LS [mm]	80
Stack length, Segments [mm]	78
LS outer diameter [mm]	100
Gear ratio	15:1
MG slip torque 2D/3D FEA [Nm]	116/106
MG volume (Active material) [l]	0.628
MG torque density, 3D FEA [Nm/l]	169
External volume added [l]	1.25

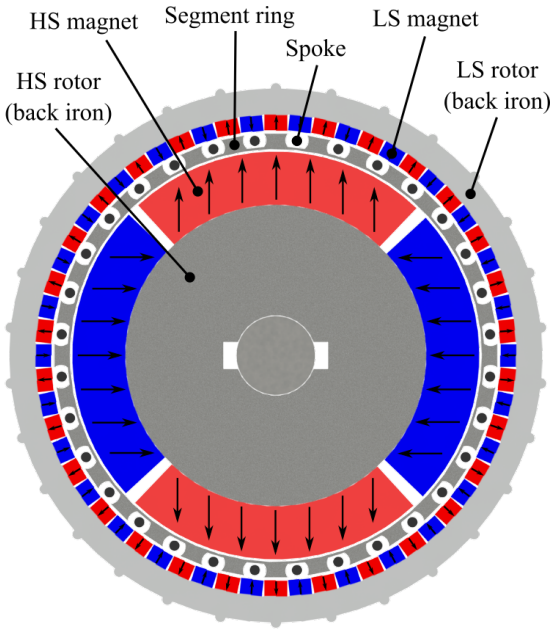

Fig. 3. Cross section of final MG with all practical mechanical aspects applied. Magnetisation indicated by arrows.

A large challenge in the development of the MG drive is the integration and system design. The most challenging part is the segment ring. The thickness of the bridge in this demonstrator is as small as it is possible to manufacture to minimise the influence on the slip torque although it plays an important role in the structural rigidity of the segment ring. The lamination stack is bonded together with a bonding varnish. By doing this, the segment ring becomes a structural component contributing to a segment ring strong enough to transfer the torque. To fix the segment ring in the MG, the original idea has been to mount the segment lamination stack in an injection molding tool and then overmold the stack, hereby filling the voids between segments with a polymer, and in the same operation mold flanges on each end to attach the segment ring to the aluminium flanges of the drive unit via screws. The segment ring and white polymer flanges are seen in fig. 2c. However, due to the high costs related to tooling and the uncertainty of success in the first shot, the alternative construction in fig. 4 is made. Here, two flanges with fingers fitting in between segments are milled from PEEK, and austenitic stainless steel spokes are used to clamp the lamination stack between the flanges. These spokes are furthermore protruding through the aluminium flange to which this side is mounted and fixed with nuts. Note that the spokes are only electrically short circuited in one end to avoid large circulating currents. This construction is not suitable for manufacturing on a large scale, but it will be sufficient for the demonstrator. The importance of using a nonmagnetic, nonconductive materials for structural parts in the vicinity of the segment ring to avoid reduction in slip torque and excessive rotational losses has been shown in several papers [17] [18]. The slightly shorter stack length of the segment ring is found to yield the highest slip torque, which agrees with the conclusions of [19].

Like the segment ring, the back iron for the LS rotor is based on a bonded stack of laminations. The outside of this stack is provided with half round details to transfer the torque from the laminations to the white sprocket made from Polyoxymethylen (POM), see fig. 5. The inside is provided with a series of flat sections and protrusions to assist correct placement and a good glue joints between LS magnets and back iron. Each LS pole is divided into 4 sections in the axial direction as the magnets are very thin, and each pole is furthermore segmented in the tangential direction for reduced magnet loss. Fig. 5 further show the direction of magnetisation for 5 LS magnets with arrows.

In addition to the construction and manufacturing of the segment ring itself, having three concentric rotors are further complicating the mechanical design of an MG compared to a traditional electrical machine. If all three rotors are positioned using a set of end shields, the axial length of the MG which is not actively contributing to torque transfer can become fairly large. In the case of this drive unit, the axial length is reduced by using bearings large enough to enclose the LS rotor and the segment ring. This way, all three rotors can be attached to the two flanges that constitutes the drive unit. As the maximum LS speed is 298 rpm, the mechanical losses in the large bearings will be small. The HS rotor on the other hand can still be suspended in bearings with a smaller diameter to keep these bearing losses low.

The inner diameter of the PMSM stator is kept as large as possible to increase the surface area which transfer the heat generated by the copper- and core-losses in the stator. As

the segment ring has been designed with the spokes coming though the motor flange, the depth of the stator slot is limited. If the total length of the drive unit is to be kept as short as possible, the winding will interfere with the spokes if the diameter on the bottom of the slots is to small.

The final motor specifications are seen in table III and the cross section is seen in fig. 6. The assembled demonstrator is seen in fig. 7 with the chain partly removed. The gray enclosure on the side contains the electrical connections for the PMSM. The gray wire hanging below the drive unit is for the rotational encoder which is installed on the left side for test purposes and validation.

IV. Evaluation

In this section the results of the following tests are presented:

- Rotational loss of PMSM
- Thermal test of PMSM
- Rotational loss of drive unit
- Cogging torque and vibrations
- Slip torque of MG
- Efficiency and comparison

Through these tests, the PMSM is driven by a standard frequency converter with encoder feedback.

A. Rotational loss and thermal test of PMSM

The rotational losses of the PMSM is evaluated via retardation tests. In these tests, the PMSM is accelerated to full speed (4500 rpm) and the power to the PMSM is cut so that the windings are open circuit. Time and speed are then continuously monitored and logged until standstill of the PMSM and the data is used together with the rotor inertia to calculate the power loss. The results are seen in fig. 8 and they show rotational losses for the rotor with original magnets which are quite high. To learn more about the location of the rotational losses, the PMSM was run no-load at different speeds while recording the rotor temperature with a thermal camera. The rotor temperature were compared to the temperature of the stator and aluminium flange on which the stator is mounted which were recorded with thermocouples. It was seen that the temperature of the rotor were high compared to the other components, indicating large eddy current losses in the rotor magnets. Another rotor has been build where the magnets are segmented axially into 5 pieces, and the retardation tests are repeated. The segmentation reduces the rotational losses with 75-90 W at 4500 rpm, depending on magnet temperature, which very strongly indicates that significant eddy current losses are present in the original magnets. The sensitivity to eddy current losses is further shown by a test where the PMSM is running without load at 1000 rpm with the original rotor until steady state temperature is reached. The test is performed

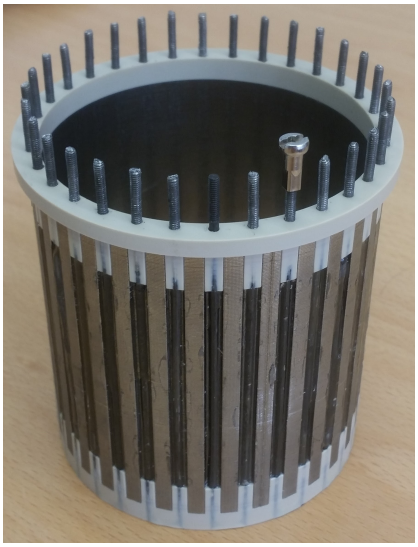

Fig. 4. Segmentring. The spokes are used to clamp the stack between the PEEK end-rings and to fix the segment ring to the motor flange.

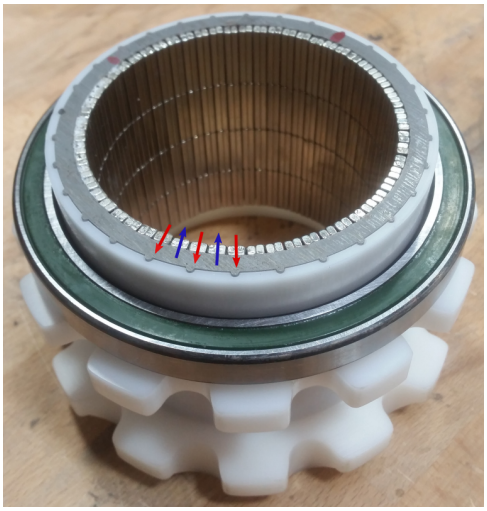

Fig. 5. The LS rotor is fixed inside the white POM sprocket, and the torque is transferred via the half round details seen on the outside of the back iron. Direction of magnetisation is shown for 5 LS magnets with arrows.

TABLE III
Final dimensions of PMSM

Outer rotor diameter [mm]	144
Inner stator diameter [mm]	74
Pole pairs	5
Number of slots	12
Slot opening [mm]	4
Magnet thickness [mm]	4
Magnet ratio	0.96
Back iron thickness [mm]	5
Stator teeth thickness [mm]	10
Stator yoke thickness [mm]	6.5
Stack length [mm]	22
Magnet grade	N3830
Air gap [mm]	0.4
Slot area [mm^2]	300
Fill factor	0.39
Nominal torque @ 5 A/mm^2 [Nm]	6.7
Nominal torque density @ 5 A/mm^2 [Nm/l]	18.7

This article has been accepted for publication in a future issue of this journal, but has not been fully edited. Content may change prior to final publication. Citation information: DOI 10.1109/TIA.2020.2977877, IEEE Transactions on Industry Applications

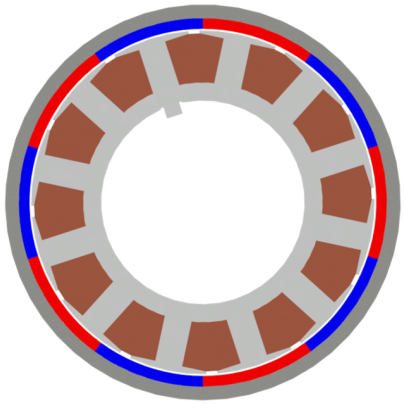

Fig. 6. Cross section of PMSM.

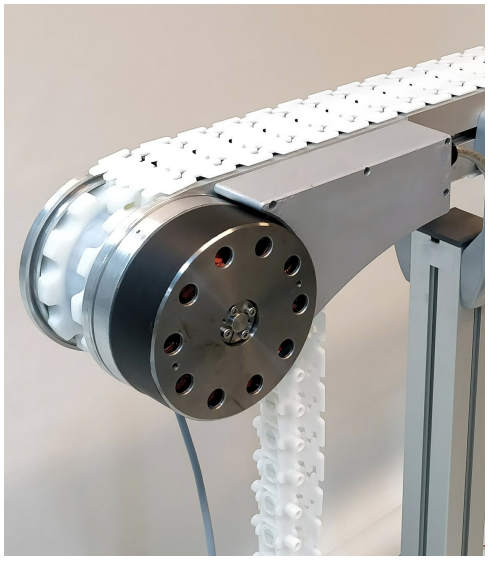

Fig. 7. Demonstrator assembled and mount to the test track. Chain is partly removed to reveal the sprocket.

with two different inverter carrier wave frequencies of 5 and 10 kHz, where the rotor reaches a temperature of 53°C and 45°C respectively. As the inductance of the PMSM is quite low, the overlaying current ripple of the motor currents is large enough to induce noticeable additional eddy current losses.

To get an indication of the thermal properties of the PMSM stator with respect to dissipation of copper loss, thermal tests are performed with a DC current through the series connected phase windings. The copper temperature is measured with two different methods, one being a thermocouple in an end winding and the other being an indirect method where the temperature rise is found from the increase in winding resistance. The first gives a point temperature in the end winding and the latter gives an average winding temperature. The first test is performed with a current density of 5 A/mm^2 which corresponds to the peak torque of 6.7 Nm that must be delivered during a limited start-up period. The second test is performed at 6 A/mm^2. As the PMSM rotor and electrical

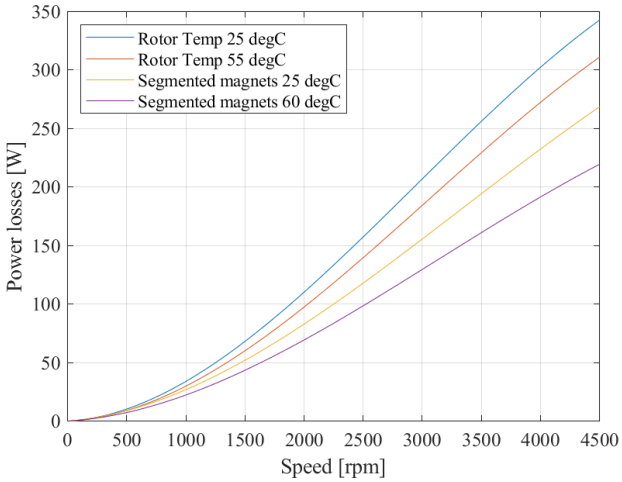

Fig. 8. Rotational loss of PMSM as a function of speed. Original and segmented magnets tested at different temperatures.

connections must be enclosed for safety on the final drive unit the test with 6 A/mm^2 is repeated with printed ABS dummy enclosures installed to see the influence. The measured steady state temperatures are given in table IV.

The average temperatures in table IV is higher than the temperature of the end winding which is unusual. However, the thermocouple is placed on the outside of the end winding, hence a lower temperature must be anticipated compared to a measurement in the center of the end winding. The resulting average temperature of 78°C at nominal current is promising, and although more sources of loss are added under real operating conditions, the additional frequency dependent losses under maximum torque conditions are limited, as maximum torque is only required below an input speed of 186 rpm. Hence, the 155 °C temperature limit of a class F winding leaves a good margin.

B. Rotational loss of drive unit

To find the rotational losses of the MG, retardation tests are repeated for the complete drive unit, and in fig. 9 the rotational loss of the PMSM, the MG and total (PMSM + MG) is shown by solid lines. The test reveals a total rotational loss of 1553 W at the maximum PMSM speed of 4500 rpm, constituted by 269 W in the PMSM and 1284 W in the MG.

The large losses are likely to be caused by eddy currents in the components surrounding the MG, induced by a magnetic leakage field. The leakage field is caused by very strong magnets on the HS rotor configured with only 4 poles and a

TABLE IV
STEADY STATE WINDING TEMPERATURE IN DC TEST.

Current density	End winding [°C]	Average [°C]
5 [A/mm^2]	69	78
6 [A/mm^2]	92	104
6 [A/mm^2] w. enclosure	100	112

This article has been accepted for publication in a future issue of this journal, but has not been fully edited. Content may change prior to final publication. Citation information: DOI 10.1109/TIA.2020.2977877, IEEE Transactions on Industry Applications

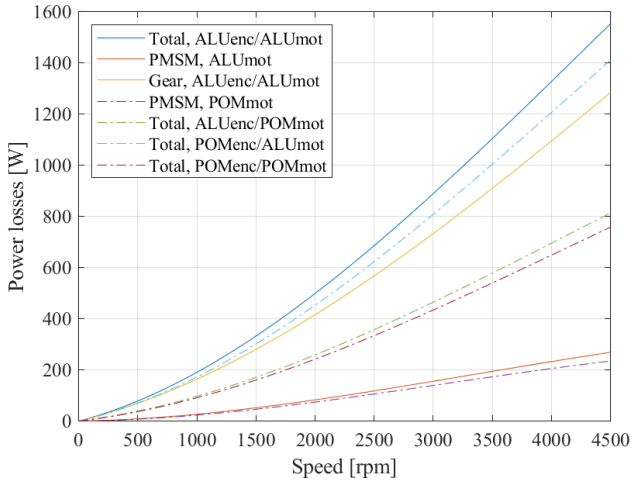

Fig. 9. Losses in surrounding components are separated by retardation tests where different electrically conducting parts are swapped with non-conducting parts.

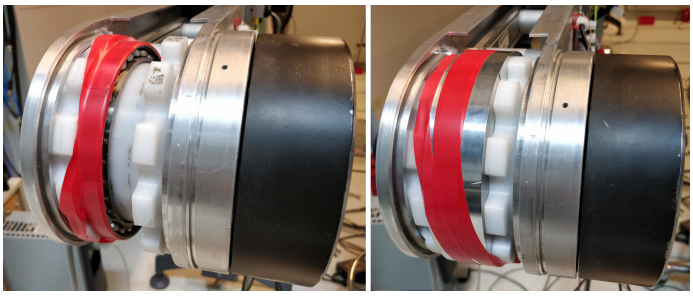

Fig. 10. Two tests performed to locate losses in motor flange. One with extra bearing and one with extra bearing + aluminium.

fairly thin LS back iron which is highly saturated, and hereby not able to contain the magnetic field. Especially the flange to which the PMSM is mounted is heating up rapidly, and in fig. 2c it is seen that this flange is overlapping the MG. To demonstrate the leakage field thesis, tests are designed to separate the loss induced by MG and PMSM in each of the major surrounding components by substituting the aluminium flanges with flanges made from POM. In fig. 9 the results of these tests are also shown. In the legend the motor flange in aluminium is called ALUmot and the encoder flange in aluminium is called ALUenc. Likewise, POM is used when a POM flange is introduced.

In addition to the large volume of aluminium placed radially outside the MG, this space also features a large bearing. To further separate the rotational loss in the motor flange, two tests are made where an additional bearing and an additional bearing together with a piece of aluminium is placed on the sprocket to determine how much the rotational loss increase, see fig. 10 for experimental setup and fig. 11 for a cross sectional cut. From these tests it is found, that at full speed, 74 W of loss is induced in the bearing and that 72 W of loss is located in the material located radially outside the LS rotor.

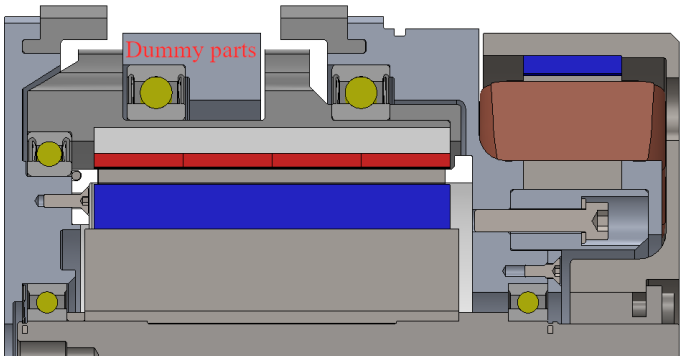

Fig. 11. Cross sectional view of upper half of the drive unit showing the additional bearing and aluminium section on the sprocket.

Table V shows the rotational loss at full speed for different flange material configurations. Gear, PMSM and total denotes if the loss is present in the MG, PMSM or the combined unit. Table VI shows losses in each drive unit component derived from the tests. The rotational loss in the active MG parts, being laminations and magnets, is found by subtracting losses in flanges, bearings and PMSM from the total loss. The mechanical loss of the large bearing is found through a bearing calculator from the manufacturer, SKF. It is clearly seen that the majority of the rotational loss is found in the motor flange and the active MG parts. From the tests with additional aluminium placed on the sprocket it was found, that only 72 W of loss was induced in this section. Also, in table V results are shown from two tests with the PMSM mounted on an aluminium flange and a POM flange. These tests show that the PMSM is inducing 34 W of loss in the aluminium flange. These losses are assumed to be induced in the same part where the 72 W were induced by the MG, as the windings are open circuit during retardation tests, hence no current is running in the windings to induce losses in the aluminium nearby. Also, the PMSM rotor back iron is quite saturated, hence leakage fields must be anticipated. If the assumptions above are correct, the remaining loss must be induced in the central parts of the motor flange between MG and PMSM.

An interesting observation is made when comparing the encoder flange loss at full speed from tests in different flange material configurations. In table VI two different losses are given, depending on how the number is derived. When comparing the rotational loss with 2 aluminium flanges with

TABLE V
ROTATIONAL LOSS AT FULL SPEED (PMSM @ 4500 RPM) FOR DIFFERENT FLANGE MATERIAL CONFIGURATIONS.

Configuration	Loss [W]
Total, ALUenc/ALUmot	1553
Total, POMenc/ALUmot	1410
Gear, ALUenc/ALUmot	1284
Total, ALUenc/POMmot	813
Total, POMenc/POMmot	758
PMSM, ALUmot	269
PMSM, POMmot	235

This article has been accepted for publication in a future issue of this journal, but has not been fully edited. Content may change prior to final publication. Citation information: DOI 10.1109/TIA.2020.2977877, IEEE Transactions on Industry Applications

TABLE VI
DERIVED ROTATIONAL LOSSES IN DRIVE UNIT COMPONENTS AT FULL SPEED (PMSM @ 4500 RPM).

Component	Loss [W]
Aluminium motor flange	666
Aluminium encoder flange	143/55
Bearing, induced	74
Bearing, mechanical	1
PMSM, on POM flange	235
Active MG parts	522

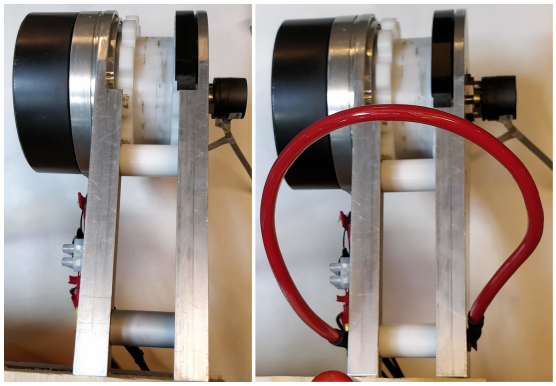

Fig. 12. Left: Upper spacer in POM and lower spacer in aluminium. Right: Both spacers in POM, flanges connected electrically by wire.

the rotational loss were the encoder flange is made from POM ("Comparison 1"), there is a difference of 143 W. However, if the rotational loss in a configuration with aluminum encoder flange / POM motor flange is compared with a configuration with both flange made from POM ("Comparison 2"), a difference of 55 W is obtained. The difference may be explained by losses induced in a current loop constituted by motor flange, 2 spacers between flanges, encoder flange, HS shaft and bearings. As this loop goes though the HS rotor, it links a varying flux which induces a voltage in the loop. To investigate this theory, retardation tests are performed with one spacer in POM and the other changing between aluminium and POM to break the electrical path. A configuration with to different spacer materials is seen to the left in fig. 12. Three tests in each configuration is made, and at full speed, the average loss of the tests with electrically isolated flanges is 17 W lower compared to the average loss with electrically connected flanges. To further confirm this result, the two otherwise electrically isolated flanges are connected with a wire in which the current is measured at full speed, the wire is seen to the right in fig. 12 and the measured waveform is seen in fig. 13. The frequency of the current matches the frequency of the magnetic field on the HS rotor. This confirms the hypothesis with a current induced in the path described, and the retardation tests indicate, that a loss due to this current is present. This observation is not only relevant to reduce the rotational losses in the MG. It also shows that a current is running through the HS bearings which may be even more important, as bearing currents are known to reduce bearing life and hence must be avoided [20].

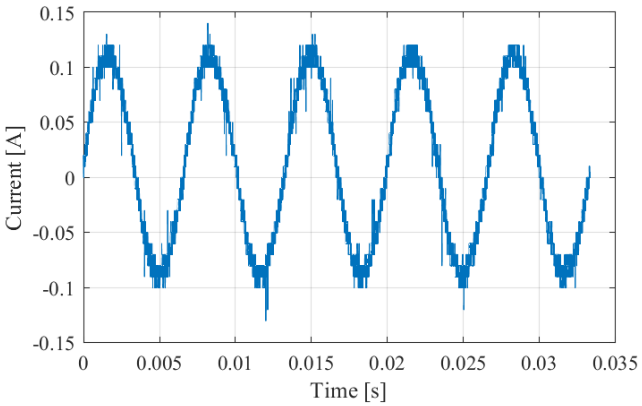

Fig. 13. Current in spacer at full speed.

C. Cogging torque and vibrations

Turning the HS shaft of the MG reveals a large cogging torque. The cogging torque has an amplitude of 2.5 Nm which is measured by mounting an arm to the HS rotor and pulling at a certain radius with a force transducer. This is very close to what can be predicted by the FE model with the LS rotor in neutral position, see fig. 14. The cogging torque is directly transferred as vibrations and acoustic noise to the conveyor system. The correlation between cogging frequency and vibrations is established by measuring the vibrations on the main beam on which the conveyor chain is riding, as well as on the chain itself. The vibrations are measured by a 2-axis accelerometer with a sample frequency of 10 kHz. From an FFT analysis of the vibrations it is clearly seen that the main component in the spectrum is coinciding with the cogging frequency. This is not acceptable and must be avoided on a future version. The cogging torque is a result of the pole configuration and the integer gear ratio. The least common denominator between HS pole pairs and number of steel segments in the segment ring is 32 which is too low, and this issue must be seen as an inadvertent mistake during design. If the number of segments is altered to 33 and the

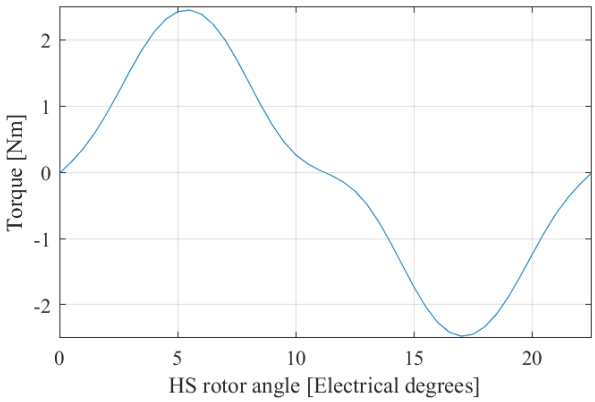

Fig. 14. Calculated cogging torque of HS rotor from the 2D FE model.

This article has been accepted for publication in a future issue of this journal, but has not been fully edited. Content may change prior to final publication. Citation information: DOI 10.1109/TIA.2020.2977877, IEEE Transactions on Industry Applications

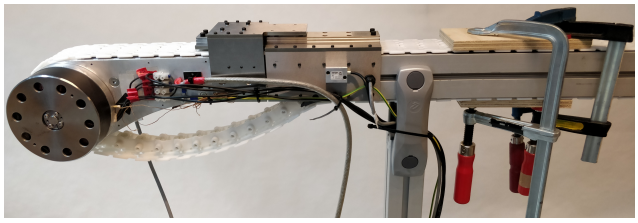

Fig. 15. Test setup for measuring slip torque.

number of LS pole pairs is increased to 31, the torque ripple is decreased to 0.05 Nm. According to 2D FEA the slip torque is reduced by 0.49 Nm which is acceptable. According to [21] the use of an uneven number of segments may result in unbalanced radial forces. This is indeed the case, as an unbalanced radial force on the segment ring of 75 N appears, however, this is low and may be allowable. In any case, by changing the pole and segment configuration there is a straight forward solution to the problem in a future version.

D. Slip torque of MG

The slip torque of the MG is not readily measurable as no shaft is present on the LS rotor. However, the LS torque can be derived from the chain tension. The test setup seen in fig. 15 has been build to measure the slip torque.

A linear guide rail constrains the motion of the drive unit in relation to the main beam of the conveyor system. Only movement in the chain direction is possible, and the forces in this direction between drive unit and main beam goes through a load cell. The chain is fixed on the main beam by the clamps, and the HS rotor is rotated until slip occurs. In fig. 16 the torque from the test of slip torque is seen. Maximum torque achieved is 89 Nm.

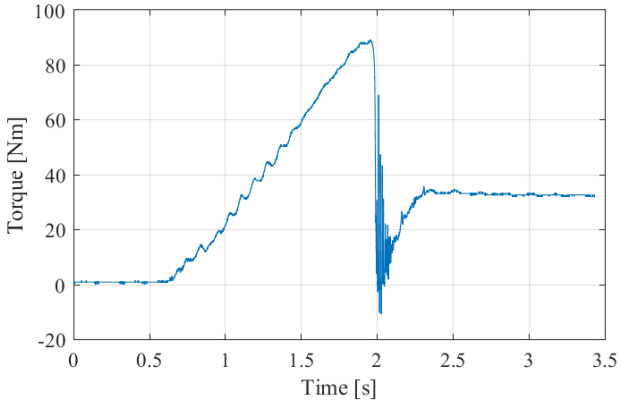

Fig. 16. Measured LS torque from slip torque test.

From 3D FEM, 106 Nm was expected and the deviation may be attributed to a couple of sources of error. The BH curve for the laminations in the MG is only known up to 2.1 T. As especially the LS back iron is under very hard saturation, above 2.4 T, the extrapolation of the BH curve has influence on the result. Also, when modeling the MG, a homogeneous air gap of 0.4 mm has been used. However, in the demonstrator, half of the air gap is 0.4 mm and the other half is 0.5 mm due to the segmented LS magnets and the way they are physically positioned, see fig. 5. Also, as the LS magnets have a rectangular cross section, air pockets are formed between the LS poles, hence less magnet material is present in the real world. When modeling the exact LS rotor geometry in 2D, the slip torque is reduced by 4.5 Nm

A measured slip torque of 89 Nm yields an actual torque density of 142 Nm/l for the active part of the MG. To close the loop and to compare the chosen semi-integrated topology to the external topology in fig. 2b the volume which is essentially added to the original drive unit in fig. 1 is evaluated. The semi-integrated solution adds 1.25 liters which primarily consist of PMSM and aluminium structure. The torque density of this external volume is 71.2 Nm/l which can be used to compare the semi-integrated topology to the external topology. To the best knowledge of the authors, an actual torque density of 71.2 Nm/l for the total volume has not been published for an MIPMG. As an example, the MIPMG in [14] has a torque density of 99.7 Nm/l for the active materials, however, the torque density decreases to 63.9 Nm/l when the total volume is taken into account. Hence by choosing topology c) the most compact solution is obtained. On top of that, topology c) has a large benefit of the thermal decoupling between MG and PMSM as discussed.

E. Efficiency and comparison

The efficiency is measured for the demonstrator and compared to the efficiency of an existing commercial low speed / high torque drive. The efficiency is measured as a system efficiency, given by eq. (1).

$$\eta = \frac{P_{chain}}{P_{grid}} \tag{1}$$

P_{chain} is obtained as the product of the chain force and the chain speed, which is measured with an encoder wheel. P_{grid} is measured with a power analyser.

The commercial drive consists of an induction machine geared with a worm gear. The induction machine is driven by a frequency converter directly mounted to the motor. The standby power consumption of this combination is 3 W while the standby power consumption of the frequency converter used to drive the demonstrator is 15 W due to many additional functionalities. Hereby the commercial drive in the comparison will have some advantages.

Fig. 17 shows the efficiency map for the demonstrator. The large rotational losses of the demonstrator makes it undesirable to run it at high speed, hence the maximum LS speed is limited to 52 rpm which is the same as the maximum speed of the commercial drive. The peak efficiency of the demonstrator is 59.9%. The negative slope of the contour lines at low speed show the low dependency of magnetic gears on load.

Fig. 18 shows the efficiency map of the commercial drive. The peak efficiency in the operating area of this drive is 37.7%. Even though the rotational losses of the magnetically geared demonstrator has been shown to be very large, the efficiency is

This article has been accepted for publication in a future issue of this journal, but has not been fully edited. Content may change prior to final publication. Citation information: DOI 10.1109/TIA.2020.2977877, IEEE Transactions on Industry Applications

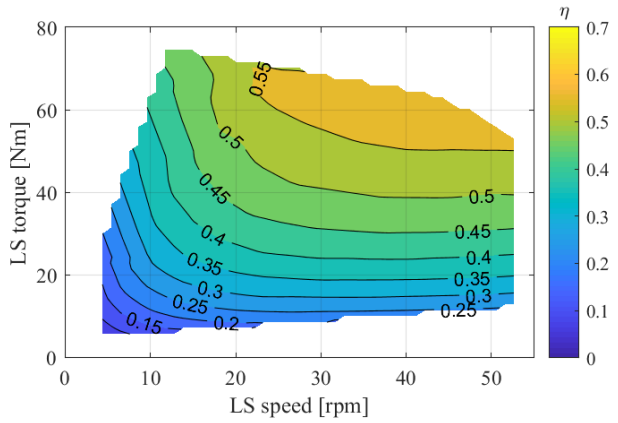

Fig. 17. Efficiency map of demonstrator.

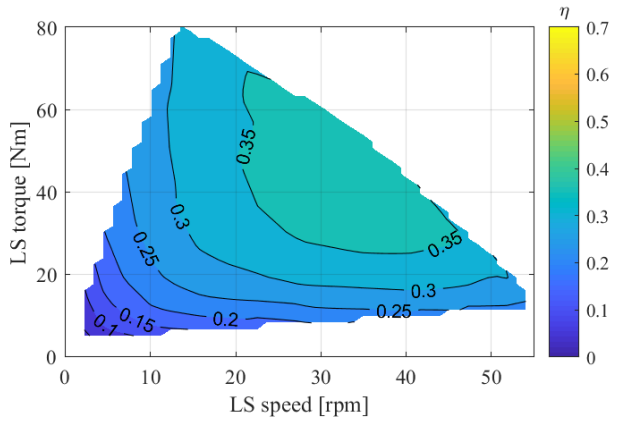

Fig. 18. Efficiency of current low speed / high torque drive unit.

overall significantly higher than the commercial drive, and the peak efficiency of the demonstrator is 22.2 percentage points, or 58.9%, higher. In addition, when mounted to the shaft of the drive unit seen in fig. 1 the commercial drive adds 11.6 liters of volume to the system compared to 1.25 liters for the demonstrator. Both volumes excludes the frequency converter.

V. Conclusion

This paper presents a magnetic gear highly integrated with a PMSM into a conveyor chain drive unit with the aim of replacing the existing solution comprised of several combinations of line fed induction machines and mechanical gears required to obtain the torque and speed characteristics for specific applications. A semi-integrated solution is chosen where the MG is inside the sprocket driving the chain, and the PMSM is on the side of the drive unit. The new drive unit is much more compact than the current motor/gear combination and a measured output torque of 89 Nm is obtained which fulfills the continuous torque requirement of 80.9 Nm, but is 11 Nm lower than the peak torque requirement of 100 Nm. A measured volumetric torque density of 142 Nm/l is obtained for the active parts of the MG.

Large rotational losses are present in the MG and PMSM. The origin of these losses are mainly surrounding aluminium flanges and MG components. Also, a bad pole configuration has been chosen with a large cogging torque as a result. However, despite the large losses, the efficiency map of the drive unit show good tendencies compared to a presently used commercial drive unit. The efficiency of the demonstrator in general is significantly better, and the peak efficiency is 22.2 percentage points higher compared to the commercial drive unit, while reducing the additional volume added to the original drive unit from 11.6 liters to 1.25 liters. The issues with losses and cogging torque can be solved, and the highly integrated drive unit generally shows promising results.

References

[1] K. Atallah, D. Howe, "A novel high-performance magnetic gear", IEEE Transactions on Magnetics, Volume 37, Pages 2844-2846, 2001

[2] T. B. Martin, "Magnetic transmission", april 1968, US Patent 3,378,710

[3] P.O. Rasmussen, T.O. Andersen, F.T. Joergensen, O. Nielsen, "Development of a high performance magnetic gear", 38th IAS Annual Meeting on Conference Record of the Industry Applications Conference, Volume 3, Pages 1696-1702, 2003

[4] K. Atallah, S. D. Calverley, D. Howe, "Design, analysis and realisation of a high-perfomance magnetic gear", IEEE Proceedings-Electric Power Applications, Volume 151, Pages 135-143, 2004

[5] S. Mezani, K. Atallah, D. Howe, "A high-performance axial-field magnetic gear", Journal of Applied Physics, Volume 99, 2006

[6] Cheng-Chi Huang, Mi-Ching Tsai, D.G. Dorrell, Bor-Jeng Lin, "Development of a magnetic planetary gearbox", IEEE Transactions on Magnetics, Volume 44, Pages 403-412, 2008

[7] F. T. Jørgensen, T. O. Andersen, P. O. Rasmussen, "The cycloid permanent magnetic gear", IEEE Transactions on Industry Applications, Volume 44, Pages 1659-1665, 2008

[8] J. Rens, K. Atallah, S. D. Calverley, D. Howe, "A novel magnetic harmonic gear", IEEE Transactions on Industry Applications, Volume 46, Pages 206-212, 2010

[9] L. Jian, K. T. Chau, "A coaxial magnetic gear with halbach permanent-magnet arrays", IEEE Transactions on Energy Conversion, Volume 25, Pages 319-328, 2010

[10] K. T. Chau, D. Zhang, J. Z. Jiang, C. Liu, Y. Zhang, "Design of a magnetic-geared outer-rotor permanent-magnet brushless motor for electric vehicles", IEEE Transactions on Magnetics, Volume 43, Pages 2504-2506, 2007

[11] P. O. Rasmussen, H. H. Mortensen, T. N. Matzen, T. M. Jahns, H. A.Toliyat, "Motor integrated permanent magnet gear with a wide torque-speed range", IEEE Energy Conversion Congress and Exposition, Pages 1510-1518, 2009

[12] K. Atallah, J. Rens, S. Mezani, D. Howe, "A novel "pseudo" direct-drive brushless permanent magnet machine", IEEE Transactions on Magnetics, Volume 44, Pages 4349-4352, 2008

[13] K. K. Uppalapati, W. Bomela, J. Z. Bird, M. Calvin, J. Wright, "Construction of a low speed flux focusing magnetic gear", IEEE Energy Conversion Congress and Exposition, Pages 2178-2184, 2013

[14] T. V. Frandsen, L. Mathe, N. I. Berg, R. K. Holm, T. N. Matzen, P. O. Rasmussen, K. K. Jensen, "Motor integrated permanent magnet gear in a battery electrical vehicle", IEEE Transactions on Industry Applications, Volume 51, Pages 1516-1525, 2015

[15] S. S. Nielsen, R. K. Holm, P. O. Rasmussen "Conveyor System with a Highly Integrated Permanent Magnet Gear and Motor", 2018 IEEE Energy Conversion Congress and Exposition (ECCE), Pages 2359-2366, 2018

[16] N. W. Frank, H. A. Toliyat, "Analysis of the concentric planetary magnetic gear with strengthened stator and interior permanent magnet (IPM) inner rotor", IEEE Transaction on Industry Applications, Volume 47, Pages 2977-2984, 2010

[17] S. Gerber, R-J. Wang, "Evaluation of a prototype magnetic gear", Proceedings of the IEEE International Conference on Industrial Technology, Pages 319-324, 2013

[18] T. V. Frandsen, P. O. Rasmussen, "Practical investigation of end effect losses in a motor integrated permanent magnet gear", IEEE Energy Conversion Congress and Exposition, Pages 4425-4432, 2015
[19] S. Gerber, R-J. Wang, "Analysis of the end-effects in magnetic gears and magnetically geared machines", International Conference on Electrical Machines, Pages 396-402, 2014
[20] P. L. Alger and H. W. Samson, "Shaft currents in electric machines", Journal of the American Institute of Electrical Engineers, Pages 1325-1334, 1923
[21] M. Johnson, M. C. Gardner, H. A. Toliyat, S. Englebretson, W. Ouyang, C. Tschida, "Design, Construction, and Analysis of a Large-Scale Inner Stator Radial Flux Magnetically Geared Generator for Wave Energy Conversion", IEEE Transactions on Industry Applications, Pages 3305-3314, 2018

Simon Staal Nielsen Simon Staal Nielsen received his M.Sc. degree in Electromechanical Systems Design in 2015 from Aalborg University. He since worked as a research assistant for 3 years with switched reluctance machines, power electronics and magnetic gears. He is currently working towards his Ph.D. degree concerning systems design and implementation of magnetic gears, electric machines and power electronics at the Department of Energy Technology on Aalborg University.

Rasmus Koldborg Holm Rasmus Koldborg Holm was born in 1986. He received the M.Sc. degree in electromechanical engineering from Aalborg University, Aalborg, Denmark, in 2012. The title of his master's thesis project was "Design of a Magnetic Lead Screw for Wave Energy Conversion." He since continued his work on magnetic lead screws and has also done some work regarding magnetic gears. He is currently working in the field of magnetic lead screws with the Department of Energy Technology, Aalborg University.

Peter Omand Rasmussen Peter Omand Rasmussen received his M.Sc.E.E and Ph.D. degrees from Aalborg University, Aalborg, Denmark, in 1995 and 2001 respectively. In 1998 he became Assistant Professor, and in 2002 he became Associate Professor at the Department of Energy Technology at Aalborg University. His research areas are the design and control of switched reluctance machines, permanent magnet machines, and magnetic gears.